International Journal of Applied Earth Observation and Geoinformation 46 (2016) 1–12

Contents lists available at ScienceDirect

International Journal of Applied Earth Observation and Geoinformation

journal homepage: www.elsevier.com/locate/jag

Mapping paddy rice planting area in rice-wetland coexistent areas through analysis of Landsat 8 OLI and MODIS images

Yuting Zhou [a], Xiangming Xiao [a,b,*], Yuanwei Qin [a], Jinwei Dong [a], Geli Zhang [a], Weili Kou [c], Cui Jin [a], Jie Wang [a], Xiangping Li [b]

[a] Department of Microbiology and Plant Biology, Center for Spatial Analysis, University of Oklahoma, Norman, OK73019, USA
[b] Institute of Biodiversity Science, Fudan University, Shanghai 200433, China
[c] Southwest Forestry University, Kunming, Yunnan 650224, China

ARTICLE INFO

Article history:
Received 3 July 2015
Received in revised form 16 October 2015
Accepted 3 November 2015

Keywords:
Paddy rice
Rice-wetland coexistent areas
Landsat 8
MODIS
Phenology-based algorithm

ABSTRACT

Accurate and up-to-date information on the spatial distribution of paddy rice fields is necessary for the studies of trace gas emissions, water source management, and food security. The phenology-based paddy rice mapping algorithm, which identifies the unique flooding stage of paddy rice, has been widely used. However, identification and mapping of paddy rice in rice-wetland coexistent areas is still a challenging task. In this study, we found that the flooding/transplanting periods of paddy rice and natural wetlands were different. The natural wetlands flood earlier and have a shorter duration than paddy rice in the Panjin Plain, a temperate region in China. We used this asynchronous flooding stage to extract the paddy rice planting area from the rice-wetland coexistent area. MODIS Land Surface Temperature (LST) data was used to derive the temperature-defined plant growing season. Landsat 8 OLI imagery was used to detect the flooding signal and then paddy rice was extracted using the difference in flooding stages between paddy rice and natural wetlands. The resultant paddy rice map was evaluated with in-situ ground-truth data and Google Earth images. The estimated overall accuracy and Kappa coefficient were 95% and 0.90, respectively. The spatial pattern of OLI-derived paddy rice map agrees well with the paddy rice layer from the National Land Cover Dataset from 2010 (NLCD-2010). The differences between $Rice_{Landsat}$ and $Rice_{NLCD}$ are in the range of ±20% for most 1-km grid cell. The results of this study demonstrate the potential of the phenology-based paddy rice mapping algorithm, via integrating MODIS and Landsat 8 OLI images, to map paddy rice fields in complex landscapes of paddy rice and natural wetland in the temperate region.

1. Introduction

Paddy rice provides the most important staple food for more than half the global population (FAO, 2013) even though it only accounts for around 11% of the world's cropland area (Matthews et al., 2001). With the rapid growth in world population, the demand for food, especially rice, is increasing, which increases pressure on land, water, and biodiversity (Beddington et al., 2012; Godfray et al., 2010). Paddy rice fields consume a large amount of water (Bouman and Tuong, 2001; Döll, 2002) and emit methane (CH_4) into the atmosphere, which plays an important role in atmospheric chemistry and climate change (Zhuang et al., 2009). The largest sources of CH_4 emissions are rice paddies (~33–40 Tg yr^{-1}) (IPCC, 2013) and natural wetlands (~177–284 Tg yr^{-1}) (Stocker et al., 2013). Information on the spatial distribution and temporal dynamics of paddy rice fields is important for the studies of trace gas emissions, management of water resources, and food security (Döll, 2002; Xiao et al., 2005, 2006). An updated and accurate paddy rice map with fine spatial resolution (e.g. 30 m) is vital for policy makers and farmers to understand and balance environmental problems (greenhouse gas emissions and water deficit issues) with rice production.

We developed a phenology-based algorithm to identify paddy rice fields based on the unique phenological feature that rice plants are first grown on flooded soils (Xiao et al., 2002a, 2005, 2006; Zhang et al., 2015). At the beginning of the growing season, the land surface is a mixture of plants and water and can be detected as flooding using spectral bands or vegetation indices that are sensitive to both water thickness (Land Surface Water Index, LSWI) and vegetation canopy (Normalized Difference Vegetation Index,

* Corresponding author at: Department of Microbiology and Plant Biology, Center for Spatial Analysis, University of Oklahoma, 101 David L. Boren Blvd., Norman, OK 73019, USA.
E-mail address: xiangming.xiao@ou.edu (X. Xiao).

http://dx.doi.org/10.1016/j.jag.2015.11.001
0303-2434/

NDVI; Enhanced Vegetation Index, EVI). Those areas where LSWI were greater than NDVI or EVI (LSWI ≥ NDVI or LSWI ≥ EVI) during the growing season were identified as paddy rice fields. This algorithm has been applied to map paddy rice fields in Eastern Jiangsu Province, China using Vegetation data (Xiao et al., 2002a) and in Southern China, Northeast China, and Southeast Asia using MODIS data (Xiao et al., 2005, 2006, Zhang et al., 2015).

However, accurate mapping of paddy rice in rice-wetland coexistent areas is still challenging since both paddy rice and natural wetlands have a flooding stage in their growing season, which often leads to misclassification of natural wetlands as paddy rice (Brisco et al., 2012; Gong et al., 2010; Xiao et al., 2005). Previous studies has used the thematic map of wetland to deal with this problem and suggested the need to develop a MODIS- or Landsat-based natural wetland mask (Jin et al., 2015; Zhang et al., 2015). A more detailed analysis of the dynamics of paddy rice and natural wetland might give us more clues to solve this problem. Furthermore, the previous phenology-based algorithm has not been applied in the temperate region using Landsat 8 data that has a finer spatial resolution than MODIS although it has been tested in other paddy rice planting areas in China (Qin et al., 2015; Wang et al., 2015). The objective of this study was to develop and test an improved method to map paddy rice in the rice-wetland coexistent areas, using MODIS and Landsat 8 OLI images. As a case study, we selected the Panjin Plain in Liaoning Province, Northeastern China, as (1) extensive natural wetlands and paddy rice are distributed throughout the area and (2) field survey data, agricultural statistical data, and other fine-resolution cropland data are available for the evaluation of a Landsat 8 OLI-derived paddy rice map.

Using multi-temporal MODIS and Landsat 8 OLI images in 2013, we examined spectral characteristics of various land cover types and applied a phenology-based algorithm to map seasonally flooded/inundated areas. Then, paddy rice fields were distinguished from natural wetland based on the observation of the different timing in flooding stages. Our algorithm focused on the flooding feature of paddy rice and utilized the asynchrony of the flooding signal in paddy rice and reed wetland. It has the potential be applied to large area using program without substantial human inputs. Other conventional classification methods (e.g. Maximum Likelihood, ISODATA, SVM, etc.) either need the prior knowledge of the land cover samples or post classification interpretation which are time consuming and labor intensive. The algorithm has the potential to generate better paddy rice results than others without considering the asynchrony of the flooding signal in paddy rice and reed wetland. The algorithm developed in this study takes advantage of the high temporal resolution (8-day) of MODIS images at 500 m spatial resolution and the high spatial resolution (30 m) of Landsat 8 OLI images at 16-day temporal resolution and may be applied to other rice-producing areas to generate a paddy rice database at 30 m spatial resolution. Such a data product would be critical for studying estimation of trace gas emissions, water sources management, wild bird migration, and food security.

2. Materials and methods

2.1. Study area

The Panjin Plain is located in the core area of the Liaohe Delta in Liaoning province, Northeast China (40.623–41.597°N,

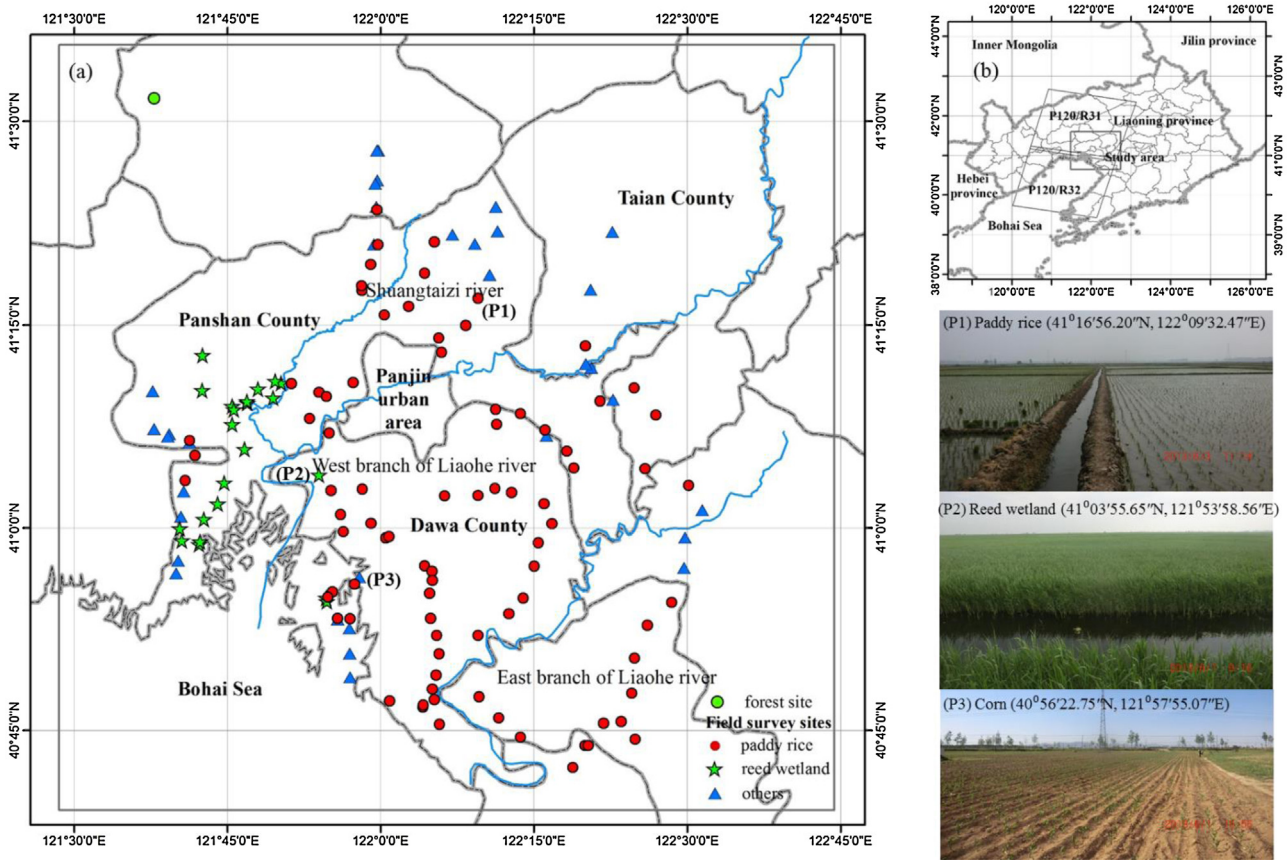

Fig. 1. (a) Location of the field surveysites in the Panjin Plain, Liaoning Province, China. The total number of sites for paddy rice, reed wetland, and others (corn, soybean, water body etc.) were 86, 21, and 34. (b) Landsat tiles (path/row)for the study area and its location in Liaoning province. (P1), (P2), and (P3) are the photos that show the paddy rice, reed wetland and corn fields.

Table 1
Landsat 8 images used in this study. Two tiles (Path120/Row31 and Path120/Row32) are combined to cover the study area. The cloud cover information of each image is given by the metadata.

DOY	Date	Cloud cover (P120/R31)	Cloud cover (P120/R32)
2013111	4/21/2013	2.86%	17.06%
2013127	5/7/2013	Only thermal bands	Only thermal bands
2013143	5/23/2013	0.14%	4.19%
2013159	6/8/2013	0.24%	22.18%
2013175	6/24/2013	75.77%	89.56%
2013191	7/10/2013	No image available	No image available
2013207	7/26/2013	3.44%	2.68%
2013223	8/11/2013	65.18%	22.06%
2013239	8/27/2013	91.32%	58.90%
2013255	9/12/2013	3.00%	23.16%
2013271	9/28/2013	48.17%	30.25%
2013287	10/14/2013	No image available	No image available
2013303	10/30/2013	1.00%	0.98%
2013319	11/15/2013	0.89%	1.36%
2013335	12/1/2013	5.59%	4.72%
2013351	12/17/2013	45.93%	47.69%

121.376–122.813°E). Four counties are included in the study area: Panshan County, Dawa County, Panjin urban area, and Taian County. The first three counties are part of Panjin City with Panjin urban area as the business and administration center and it has a smaller area than the other two. Two main streams of the Liaohe River, one of the largest rivers in Northeastern China, run through the area (Fig. 1a).

The Panjin Plain belongs to the temperate zone and has a monsoon climate (Xu et al., 2009). Annual mean temperature is ~10.6 °C. Annual precipitation is 444 mm, and most of the precipitation occurs between May and September. Forest and natural wetland are the major natural vegetation types. Paddy rice is the most important cropland in this area. Paddy rice, corn, and soybean accounted for 84%, 12%, and 4% of the total crop area in Panjin City in 2012, respectively (Liaoning Statistical Bureau, 2014, 2013).

2.2. Data

2.2.1. Landsat 8 (OLI) data and processing

Landsat 8 provides a good source for paddy rice mapping with new features that build upon its predecessors. It gets rid of the gaps problems in Landsat 7 ETM+ and has the same spatial resolution (30 m) which makes it possible to generate finer resolution paddy rice map than MODIS (Salmon et al., 2015; Zhang et al., 2015). The additional quality assessment band includes information on cloud and cirrus; ETM+ and its predecessors do not have such quality information for each pixel which might bring error in previous studies (Beddington et al., 2012; Liu et al., 2005).

We downloaded Landsat 8 data products from April to December 2013 in the Panjin Plain from the USGS EarthExplorer (http://earthexplorer.usgs.gov/). Two tiles are needed to cover the study area (Fig. 1b). A total of 26 images were used for this study (Table 1).

Each Landsat 8 OLI image was atmospherically corrected to generate surface reflectance, using the Fast Line-of-Sight Atmospheric Analysis of Spectral Hypercubes (FLASSH) (Adler-Golden et al., 1999; Matthew et al., 2000), a matured and easy to use atmospheric correction method imbedded in popular remote sensing software (e.g. ENVI). The OLI data product includes a 16-bit quality assessment (QA) file in GeoTIFF format, which contains information on clouds and cirrus. We used the Landsat-LDOPE Toolbelt to extract cloud and cirrus covered pixels from the QA file. The medium (34–66%) confidence level was used for both cloud and cirrus information detection in the QA file. Other criteria were further applied to detect cloud: when a pixel has a blue band reflectance value ≥0.2 and a positive LSWI value, it was masked as a cloudy pixel. In order to exclude the effect of cloud and cirrus, we combined these three criteria to generate a cloud mask for each image; all cloud pixels were excluded from further analysis (Xiao et al., 2006).

For each image, we calculated NDVI, EVI, and LSWI using surface reflectance from blue (ρ_{blue}), red (ρ_{red}), NIR (ρ_{nir}), and SWIR (ρ_{swir}, 1.63–1.65 μm) bands:

$$NDVI = \frac{\rho_{nir} - \rho_{red}}{\rho_{nir} + \rho_{red}} \quad (1)$$

$$EVI = G \times \frac{\rho_{nir} - \rho_{red}}{\rho_{nir} + C_1 \times \rho_{red} - C_2 \times \rho_{blue} + L} \quad (2)$$

$$LSWI = \frac{\rho_{nir} - \rho_{swir}}{\rho_{nir} + \rho_{swir}} \quad (3)$$

NDVI is related to changes of leaf area index and the amount of green biomass within the canopy (Xiao et al., 2002b), but it has some limitations including saturation under dense canopy and vulnerability to atmospheric conditions and visible soil background (Huete et al., 2002). EVI uses the blue band in combination with the red band to reduce atmospheric contamination and also has a soil background adjustment factor L. The coefficients C_1, C_2, and L are 6.0, 7.5, and 1.0, respectively, and G is a gain factor set to 2.5 (Huete et al., 2002). LSWI is sensitive to equivalent water thickness (Xiao et al., 2002a).

2.2.2. MODIS data and processing

MODIS Land Surface Temperature (LST) products provide the estimation for daytime and nighttime land surface temperature at 1-km spatial resolution (Wan et al., 2002). The 8-day LST products (MOD11A2) were used to investigate temperature dynamics at the regional level.

MODIS land surface reflectance data (MOD09A1) was used to investigate the dynamics of different land cover types. NDVI, EVI, and LSWI were calculated using the same equations mentioned in the above section. Normalized Difference Snow Index (NDSI) was also calculated from the MOD09A1 data using green and SWIR bands, which is used in snow/ice identification latter (Hall et al., 2002) to minimize the potential impact of those observations with snow/ice cover in the spring and winter.

$$NDSI = \frac{\rho_{green} - \rho_{swir}}{\rho_{green} + \rho_{swir}} \quad (4)$$

2.2.3. Crop calendar

Paddy rice seeds are sown in a small, richly nourished seed bed in mid-April, and it takes about one month for the seeds to grow up and be ready to be transplanted into flooded fields. Flooding is an important feature of paddy rice that differentiates it from other plants, including soybean, corn, and deciduous forest (Table 2). Usually, farmers irrigate the paddy rice fields at the end of April and then transplant rice plants in late May. In June and July, the rice seedlings grow quickly and cover the whole area of the field. The rice plant is mature by the end of September and harvested in October.

Plants in natural (reed) wetland begin to germinate in late April or early May when temperatures rise up to 0 °C. When reed wetland is in the leafing stage with a closed canopy in middle or late May, paddy rice fields are still in the flooding stage. The asynchrony of the paddy rice's and reed wetland's growing season phases makes it possible to distinguish them using multi-temporal satellite images.

2.2.4. Field survey data

We carried out a field survey in the study area during the period of May 31st–June 3rd, 2013, when most paddy rice fields were in the flooding/transplanting phase and reed wetland had a closed canopy. The sampling distance between two different sites was

Table 2
Phenology stages of major plants in the Panjin Plain, Liaoning Province, China. The phenology data of paddy rice, soybean, and corn were provided by China Meteorological Data Sharing Service System (http://cdc.cma.gov.cn/home.do). The phenology stages of reed wetland and deciduous forest were extracted from (Li et al., 2006) and (Yu and Zhuang, 2006), respectively.

Month	April			May			June			July			August			September			October		
Ten-day	E	M	L	E	M	L	E	M	L	E	M	L	E	M	L	E	M	L	E	M	L
Paddy rice		1	2			3	4	5				6	7		8			9	10		
Soybean				1	2	3		4		5	6							7			
Corn				1	2	3	4		5		6		7					8			
Reed wetland			1		2							3						4			
Deciduous			1		2			3										4			

Paddy rice: 1-Sowing, 2-Seeding/flooding, 3-Transplanting/flooding, 4-Reviving, 5-Tillering, 6-Booting, 7-Heading, 8-Milky maturity, 9-Mature, 10-harvesting;
Soybean: 1-Sowing, 2-Seeding, 3-The third true leaf, 4- Branches forming, 5-Flowering, 6-Pod setting 7-Mature;
Corn: 1-Sowing, 2-Seeding, 3-Three leaves, 4-Seven leaves, 5-Stem elongation, 6-Heading, 7-Milk maturity, 8-Mature;
Reed wetland: 1-Germinating, 2-Leafing, 3-Flowering, 4-Fade;
Deciduous Forest: 1-Sprouting, 2-Leafing, 3-Growing, 4-Defoliating.

3–5 km. The width and length of the field sites were larger than 100 m and of the same land cover type. The land cover types at the sites were classified as one of three: paddy rice, reed wetland or others. We considered corn, soybean, water body, or built-up to be "others" without listing all the specific land cover types because they were minor land cover types and also out of the major scope of this study. For the paddy rice sites, we went into the paddy rice field at least 60 m away from the border in each direction and took the geo-referenced photo. For the reed wetland sites, we stood on the road running through the large reed wetland area, instead of going into the center of the reed wetland by boat, limited by time and human resources. The total numbers of sites for paddy rice, reed wetland and other land cover types were 86, 21, and 34, respectively (Fig. 1a). All field survey sites were used in the validation process.

2.2.5. Other land cover datasets for inter-comparison

The National Land Cover Dataset from 2010 (NLCD-2010) at a 1:100,000 scale was generated by the Chinese Academy of Sciences through visual interpretation and digitalization of Landsat images (Liu et al., 2014; Zhang et al., 2014). Its classification scheme has six classes and 25 subclasses of land use types and includes paddy rice as one of the subclasses in the dataset. The human-computer interactive interpretation method was used to interpret the Landsat TM/ETM+ images and HJ-1 satellite images and generate vector patches of different land cover types (1:100,000 scale). Extensive field survey data were used to evaluate the accuracy of the NLCD-2010 dataset. The resultant NLCD were aggregated and rasterized to have a spatial resolution of 1-km with cell values assigned as the percentage of different land use and land cover types. In this study, the 1-km resolution paddy rice thematic map of the NLCD-2010 dataset was used for comparison with the Landsat 8 OLI-derived paddy rice map.

The Liaoning Statistical Yearbook from 2014 is a yearly summary public government report. The data is reported by the lower district level (city) to the provincial office. It contains the economic, societal, and environmental conditions of the year before the publication of the statistical yearbook (e.g. Liaoning Statistical Yearbook

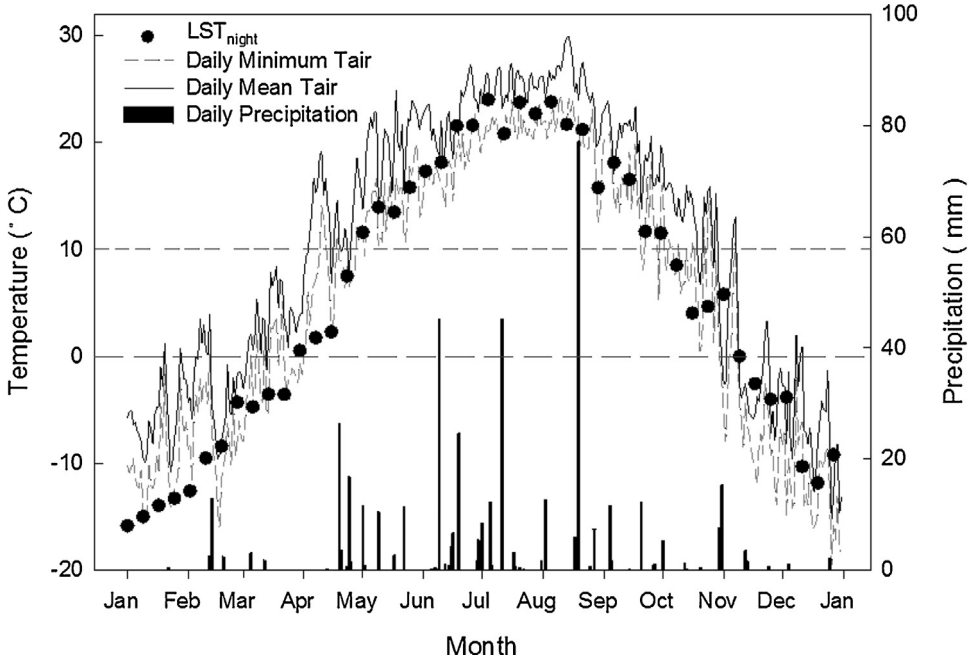

Fig. 2. Daily mean and minimum temperature, precipitation and night time land surface temperature (LST_{night}) in the Panjin Plain. Temperature and precipitation data is from the weather station located at Jin Zhou City (41.08°N, 121.07°E) and collected from China Meteorological Data Sharing Service System (http://www.escience.gov.cn/metdata/page/index.html). LST_{night} data is from MOD11A2 product for the pixel where the weather station is located in. The two dash lines denote the 0 °C and 10 °C. The weather station is not in the study area but is the closest one with data available.

from 2013 reflects the conditions of 2012). Considering the uncertainty of the statistical data, the comparison between the Landsat 8 OLI-derived paddy rice map and statistical data is coarse.

2.3. Temperature-defined plant growing season

In the Panjin Plain, the daily minimum air temperature rises above 0 °C in April (Fig. 2). It remains above 10 °C from the end of April–September. The daily minimum temperature drops below 0 °C at the end of October or the beginning of November. The temperature-defined plant growing season (0 °C threshold) runs from April to October based on the weather station data. The LST_{night} data from MODIS corresponds well with the daily minimum air temperature for the same pixel where the weather station located.

LST_{night} from MODIS rises above 0 °C usually around April 15 (Fig. 3a) in the Panjin Plain. Then, natural plants such as reeds and trees begin to grow. The regional LST_{night} map shows that the temperature rises up to 10 °C around May 9 (Fig. 3b), and paddy rice fields are in the flooding stage. LST_{night} remains above 10 °C from early May to early September (Fig. 3d) and drops to less than 10 °C at the beginning of September when paddy rice is mature and reeds enter the senescence phase. Paddy rice is harvested in October before the daily minimum temperature approaches 0 °C (Fig. 3c). The growing stages recorded by crop calendar (Table 2) matched well with the temperature-defined plant growing season from both local climate data and the LST_{night} data.

2.4. Phenology-based algorithm to identify paddy rice

2.4.1. Seasonal dynamics of vegetation indices of major land cover types from MODIS

Fig. 4 shows the seasonal dynamic of NDVI, EVI, and LSWI from MOD09A1 data for four typical land cover sites: paddy rice, reed wetland, corn, and forest. Vegetation indices of natural vegetation (Fig. 4b and Fig. 4d) increase quickly from early May. NDVI is >0.30 and EVI is >0.20 in reed wetland (Fig. 4b) in late May, indicating green-up of plants. At the same time NDVI and EVI in paddy rice (Fig. 4a) are less than 0.3 and 0.2 respectively, which suggests that transplanting has not yet started or has finished but the canopy is still open. NDVI and EVI in crops (Fig. 4a and c) increase quickly starting in late June. The LSWI values are always lower than NDVI and EVI from April to October in corn and forest while LSWI values are greater than NDVI or EVI in May and/or June in paddy rice and reed wetland, and this signal (LSWI $\geq$ NDVI or LSWI $\geq$ EVI) occurs in several continuous 8-day periods.

2.4.2. Identification of flooding/inundation signal

For the major land cover types in the study area, only paddy rice and weeds present flooding/inundation events. Some previous works suggest that LSWI $\geq$ NDVI or LSWI $\geq$ EVI coincide with flooding events (Xiao et al., 2002a, 2005, 2006). This phenomena is also present in Fig. 4(a) and (b). Those pixels identified as flooded during the whole year may be pure water or mixtures of water and plants where water information is dominant in the pixel. The seasonally flooded pixels identified in some periods of the year include seasonal water bodies, reed wetland, and paddy rice. Seasonal water bodies form during the flood season when precipitation provides a water source. This feature helps us to detect seasonal water bodies via identifying flooded pixels during plant canopies' closed period, when reed wetland and paddy rice are not flooded. After excluding permanent and seasonal water bodies from the flooding/inundated pixels, the remaining pixels are reed wetland and paddy rice.

2.4.3. The asynchronous flooding/inundation stages of paddy rice and reed wetland from MODIS and Landsat 8 OLI

The flooding signal of paddy rice can be detected in DOY 143 (5/23/2013) and DOY 159 (6/8/2013), but reed wetland was only flooded in DOY 143 (Fig. 5). The asynchronous flooding/inundation stages of paddy rice and reed wetland can be detected from both MODIS and Landsat 8 OLI data and is consistent in the points used for validation. Reed wetland is a form of natural vegetation and grows when the temperature is suitable. According to the LST_{night} data in the Panjin Plain, the temperature-defined growing season begins around April 15 (DOY 105). In DOY 159, the reed wetland canopy is closed while the paddy rice canopy is still open with a mixture of rice plants and water because the temperature-defined plant growing season for reed wetland starts about one month before paddy rice. We assumed those pixels flooded in DOY 143 but not flooded in DOY 159 were reed wetlands since the flooding signal of reed wetland lasts to the end of May and disappears before the beginning of June. Flooding pixels in DOY 159 were identified as paddy rice fields (Fig. 5).

2.4.4. Implementation of phenology-based paddy rice mapping algorithm

To implement the Landsat 8 OLI paddy rice detection algorithm at the image level, we developed a procedure (Fig. 6) by generating various masks for cloud (using the QA file, reflectance in the blue band, and LSWI as mentioned before (Section 2.2.1)), snow/ice cover, built-up and barren soil, evergreen vegetation, and permanent water bodies (Qin et al., 2015) in an effort to minimize their potential impacts.

Cloud, snow/ice, built-up and barren soil, evergreen vegetation, and permanent water bodies were excluded from identification of the flooding period. Permanent water bodies were identified based on the frequency of flooding. We assumed a pixel to be permanent water body if it was identified as water with a frequency $\geq$0.80. After applying these masks, the remainder were seasonally flooded pixels that included reed wetland and paddy rice. Paddy rice and reed wetland were then mapped according to their asynchronous flooding/inundation stages.

2.5. Accuracy assessment

Our previous study has shown that integrating the field photo library and Google Earth is reliable for generating Regions of Interest (ROIs) for land cover classification (Dong et al., 2012a, b). We combined the geo-referenced field photos collected in the field survey and high-resolution images from Google Earth to generate ROIs, following the procedure reported in a previous study (Dong et al., 2014). The image provider in the study area is Digital Globe. The images we used are mostly from April to July 2013. If there is no high resolution images during this period, we went back or forth for one year. Since our goal is to map paddy rice and the small number of other land cover type sites, we divided all the filed survey sites into two categories: paddy rice and others (including reed wetland, corn, soybean, water body etc.) to generate ROIs. A total of 141 ROIs (11, 044 pixels) were generated for product validation. Using the Landsat 8 OLI-derived paddy rice map and ROI data, we calculated the confusion matrices for paddy rice and other land cover types in an effort to obtain ROI-based validation.

2.6. Comparison with other paddy rice datasets.

The paddy rice area was summarized by county (city) from the Landsat 8 OLI-derived paddy rice map and NLCD-2010 dataset (hereafter referred to as $Rice_{Landsat}$ and $Rice_{NLCD}$). The comparison between $Rice_{Landsat}$ and $Rice_{NLCD}$ was conducted at the county level. The comparison between $Rice_{Landsat}$ and the statistical data was

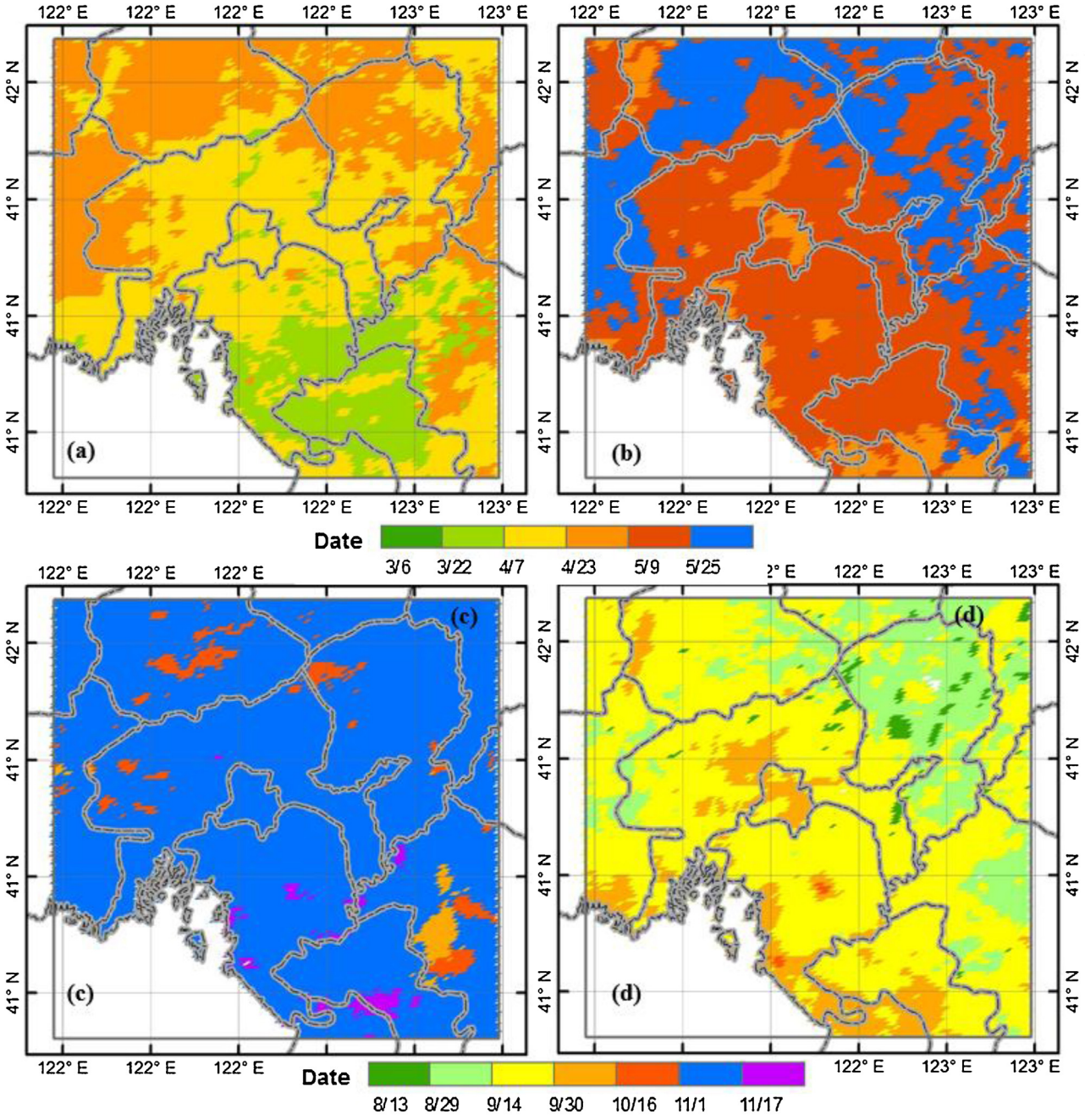

Fig. 3. Spatial distribution of temperature-defined plant growing season as delineated by LST_{night} in the Panjin Plain derived from MOD11A2 in 2013. (a) The first date with $LST_{night} >= 0\,^{\circ}C$; (b) the first date with $LST_{night} >= 10\,^{\circ}C$; (c) the end date with $LST_{night} >= 0\,^{\circ}C$; (d) the end date with $LST_{night} >= 10\,^{\circ}C$.

conducted for Panjin City as city is the smallest unit of the statistical data.

The $Rice_{Landsat}$ map is a binary (0 or 1) map with a spatial resolution of 30 m × 30 m and an area of 900 m^2 for each pixel. We counted the number of pixels with the value of 1 (indicating the existence of paddy rice) in the $Rice_{Landsat}$ map and then calculated the total area of rice by multiplying the total number of rice pixels with the area of a Landsat image pixel (900 m^2) within the area of a 1-km grid cell. Note that the grid cell in the $Rice_{NLCD}$ product has a spatial resolution of 1 km × 1 km and an area of 1 km^2, so the paddy rice area of an individual grid cell was calculated using the equation: percentage fraction × 0.01 km^2. The sum of paddy rice area in each 1-km grid cell is the total area of paddy rice in the $Rice_{NLCD}$ product.

3. Results

3.1. Spectral signature of major land cover types during and after paddy rice flooding stage

Fig. 7b1 shows the distribution of NDVI and the difference between LSWI and NDVI (LSWI-NDVI) from Landsat 8 OLI data in DOY 159, when paddy rice was still in its flooding stage but reed wetland was in its leaf stage. The LSWI-NDVI values for paddy rice and water are larger than 0, which means they are flooded. Other land cover types including reed wetland, forest, and shrub, don't show this flooding feature. The distribution of EVI and LSWI-EVI (Fig. 7c1) shows a similar pattern with NDVI and LSWI-NDVI (Fig. 7b1). The distribution of LSWI and LSWI-NDVI

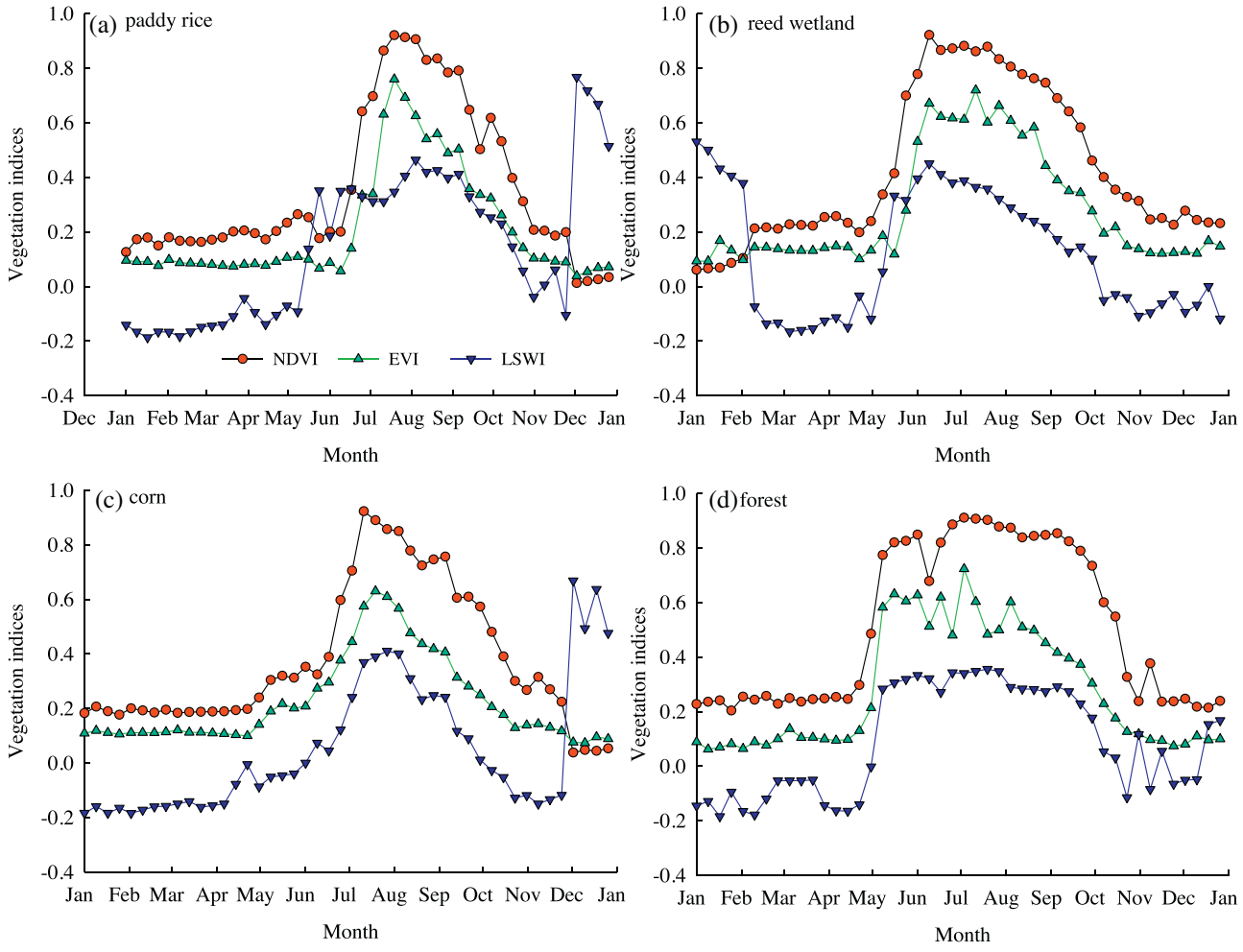

Fig. 4. The seasonal dynamics of NDVI, EVI, and LSWI of major land cover types from MOD09A1 product in 2013 (a) a paddy rice site (41.0437°N, 122.2137°E), (b) a reed wetland site (41.2127°N, 121.7095 °E), (c) a corn site (41.1159°N, 121.6550°E), and (d) a forest site (41.5279°N, 121.6303°E). All sites were selected according to the field sampling sites and were representatives of major land cover types except forest site was selected based on Google Earth image.

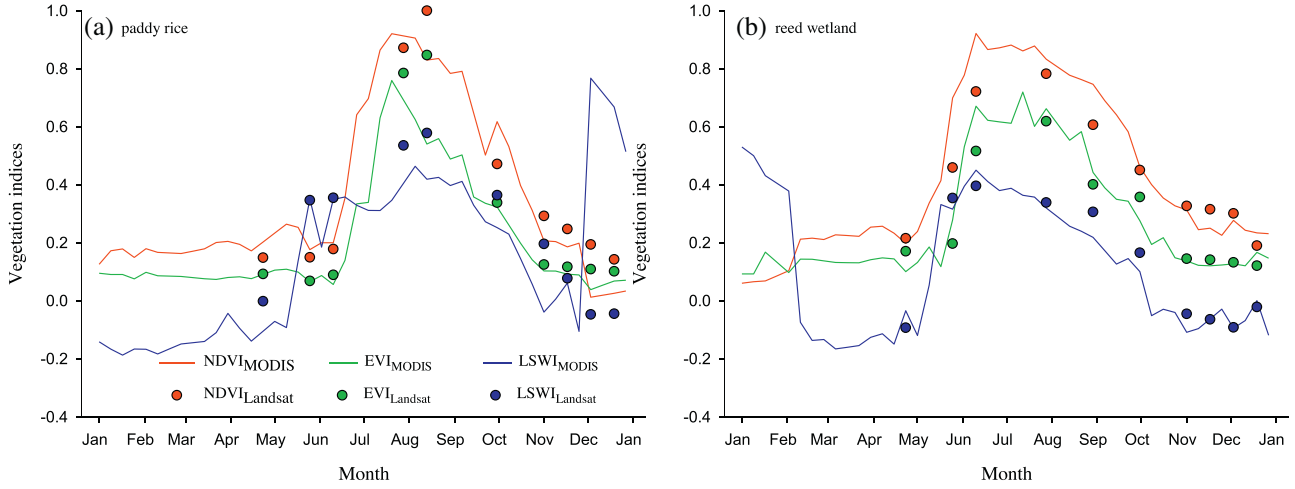

Fig. 5. The seasonal dynamics of NDVI, EVI, and LSWI from both MODIS and Landsat 8 OLI images at a paddy rice site and a reed wetland site, which were also used in Fig. 4. MODIS vegetation indices were gap-filled values while Landsat 8 OLI vegetation indices only included good observations used in this study. Black rectangles indicated the flooding periods from Landsat vegetation indices.

or LSWI-EVI have similar patterns with a clear flooding signal for paddy rice (Fig. 7d1, e1). However, the distribution of vegetation indices (NDVI, EVI, and LSWI) and the difference in vegetation indices (LSWI-NDVI, LSWI-EVI) in an image within the tillering stage (closed canopy) (DOY 207, 7/26/2013) don't have a similar pattern to DOY 159; paddy rice, reed wetland are mixed together

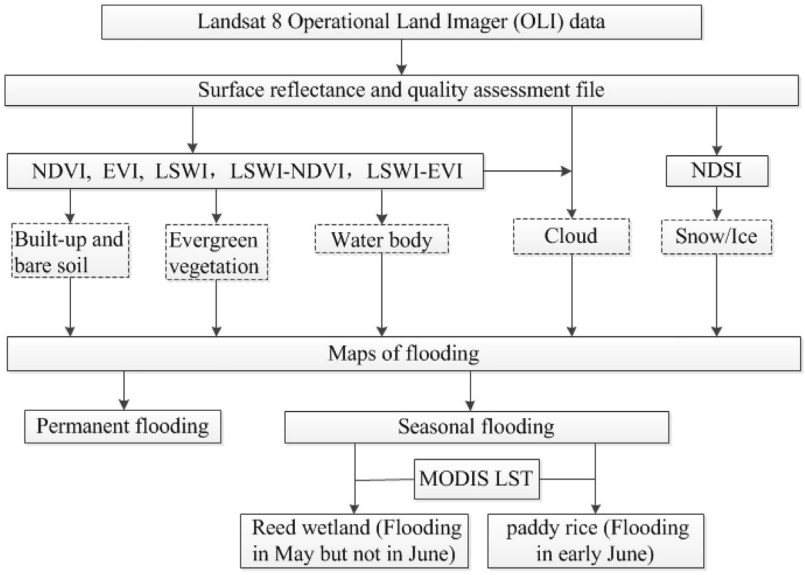

Fig. 6. A schematic diagram illustrating the implementation of the algorithm for mapping of paddy rice in the Panjin Plain from multi-temporal Landsat 8 OLI data and MODIS data.

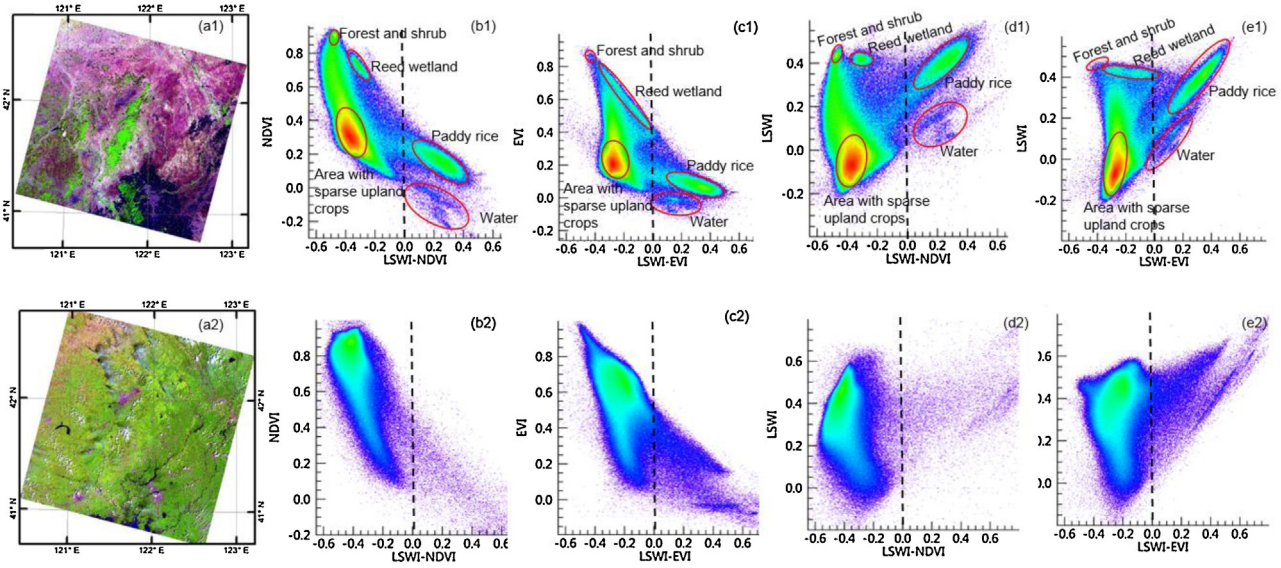

Fig. 7. The 2-D scatter plots of vegetation indices and the difference between two vegetation indices from the Landsat 8 OLI data during the paddy rice flooding period (upper panels) and the tillering period (below panels). The color density represents the number of pixels. (a) Landsat images are false composite displayed with red (SWIR), green (NIR) and blue (red), (b) NDVI versus LSWI-NDVI, (c) EVI versus LSWI-EVI, (d) LSWI versus LSWI-NDVI, and (e) LSWI versus LSWI-EVI. (For interpretation of the references to colour in this figure legend, the reader is referred to the web version of this article).

(Fig. 7 below panels). It is difficult to use images in DOY 207 to distinguish paddy rice and reed wetland since both of them have high NDVI and EVI values and are without flooding signals on that date.

3.2. Paddy rice map of the Panjin Plain from Landsat 8 OLI data

Fig. 8 shows the spatial distribution of paddy rice in the Panjin Plain from Landsat 8 OLI data. Paddy rice fields are mainly distributed in the three counties of Panjin City. No large paddy rice field appears outside of the four counties included in the study area except a relatively large one to the east of Dawa County. Paddy rice areas are mostly located along the two main streams of the Liaohe River. Some paddy rice fields are located around the Shuangtaizi River, which also runs through large reed wetland areas.

3.3. Validation of the paddy rice map derived from Landsat 8 OLI data

The classification map of paddy rice was compared with the ROIs generated based on the ground-truth data and high resolution images in Google Earth. The results indicate a very high agreement between the classification map and ground-based data for paddy rice. The overall accuracy and Kappa coefficient are, respectively, 95% and 0.90 for the ROIs based validation (Table 3). The producer's and user's accuracy for paddy rice are 93% and 91%, respectively. 91 reed wetland pixels and 221 others pixels were classified as paddy rice. Although the map of reed wetland is not good according to the field survey data, it is not mixed with paddy rice (Fig. 8). The low accuracy of the reed wetland is because some reed wetlands were never flooded during the whole year or the flooding

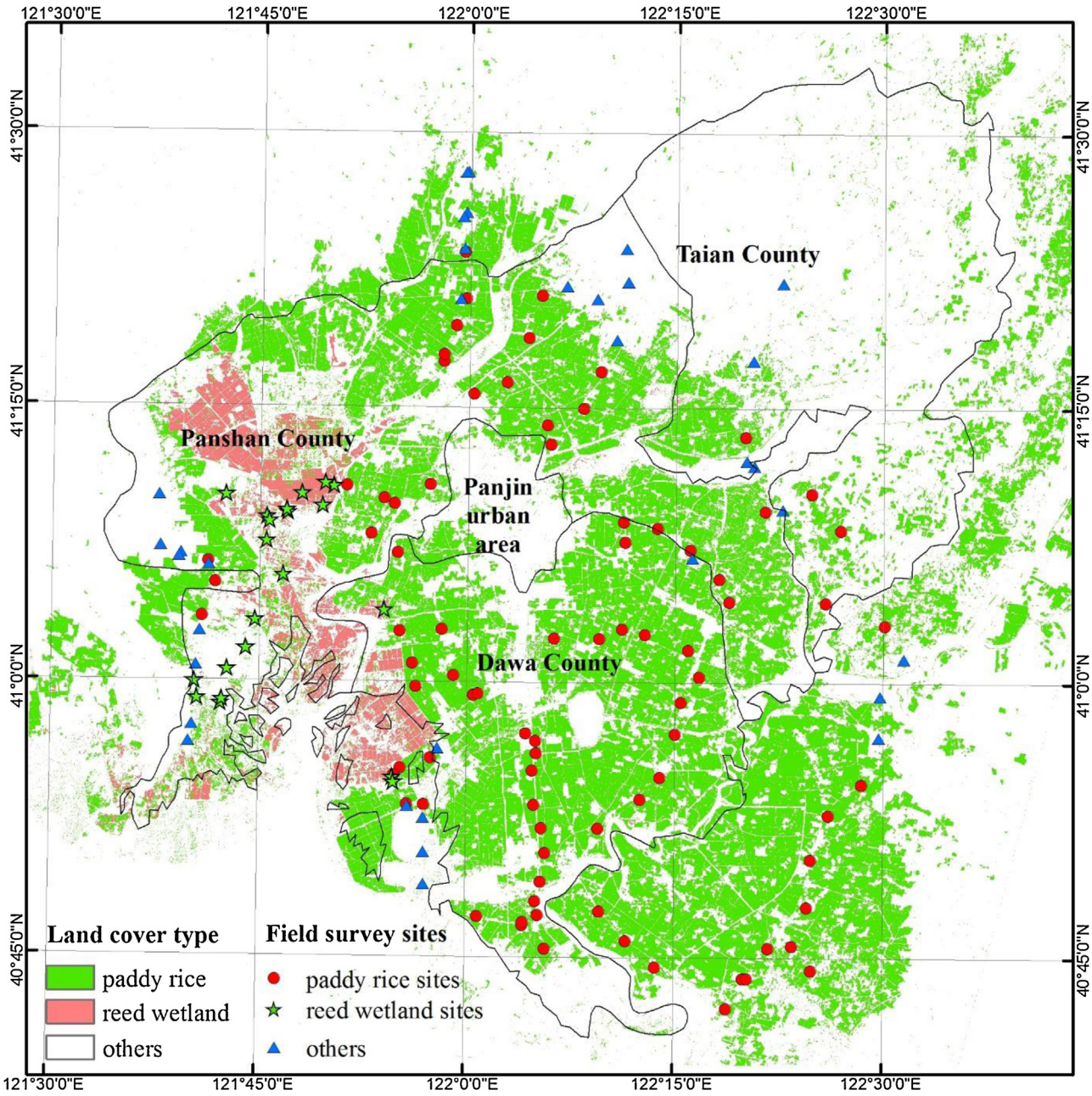

Fig. 8. The resultant paddy rice map of the Panjin Plain derived from the Landsat 8 OLI data in 2013 at 30-m spatial resolution. Field survey sites were included for reference.

signal was not captured by the Landsat images due to the 16-day revisit period and cloud and cloud shadow effect. The commission error might be because the irrigation or the flooding event in other land cover types during the paddy rice flooding/transplanting period. The omission error might be because the bad observation affected by clouds and cloud shadows and the mixed pixels of rice paddy fields and non-rice paddy fields (roads, irrigation channels, etc.).

4. Discussion

4.1. Advantages of the pixel- and phenology-based algorithm

The pixel-and phenology-based algorithm focuses on the specific phenological features of paddy rice and reed wetland in individual pixels and therefore is not dependent on other pixels' spectral features within the same image. The spectral signature of images after the flooding stage of paddy rice shows no big difference between different land cover types (Fig. 7 below panels). This indicates that the image-based clustering method might have some bias if images from canopy closed periods are used. The pixel- and phenology-based algorithm works well using MODIS data (Xiao et al., 2005, 2006; Zhang et al., 2015). The extended algorithm for Landsat 8 OLI used in this study, through analyzing the different timing of flooding stages of paddy rice and wetland works well for mapping paddy rice in rice-wetland coexistent areas in the Panjin Plain China and probably in the same latitude with similar climate. The high producer's and user's accuracy indicate the high accuracy of the Landsat 8 OLI-derived paddy rice map at 30 m resolution. However, the phenology of paddy rice and wetland should be stud-

Table 3
The confusion matrix between the $Rice_{Landsat}$ in the Panjin Plain and ROIs derived from geo-reference field photos in the field survey and high resolution images in Google Earth.

	Class	Ground truth (GT) samples (pixels)				
		Paddy rice	Others	Total classified pixels	User Acc. (%)	Commission errors (%)
Classification	Paddy rice	3322	312	3634	91	9
	Others	263	7147	7410	96	4
	Total GT pixels	3585	7459	11044		
	Pro.Acc. (%)	93	96			
	Omission errors (%)	7	5			

ied to identify the difference of flooding stages before utilizing this algorithm in other locations with different climate system.

4.2. Comparison of Landsat 8 OLI-derived rice map with other products

The spatial pattern of paddy rice from $Rice_{Landsat}$ (Fig. 9a) is very similar to that of the NLCD-2010 reference dataset (Fig. 9b), though the former shows more heterogeneity. There are some notable differences between the $Rice_{Landat}$ and $Rice_{NLCD}$ map. First, in the western part of the study area, $Rice_{Landsat}$ identifies some scattered paddy rice fields while the $Rice_{NLCD}$ product reports almost no rice fields in this region. Farmers converted reed wetlands into the paddy rice files seen in the western part of the $Rice_{Landsat}$ map to increase their income according to the observation of our field survey. Second, paddy rice fields in the Panjin urban area are smaller in the $Rice_{Landsat}$ map than in the $Rice_{NLCD}$ product. The reason is the rapid urbanization of the city area. We can see that the size of Panjin urban area in the $Rice_{Landsat}$ map was larger than in the $Rice_{NLCD}$ map. According to the statistical yearbook in Liaoning province from 2010 to 2013, the built-up area in Panjin City increased from 58.9 km^2 to 69.6 km^2. The spatial pattern of the differences between Landsat 8 $Rice_{Landsat}$ and $Rice_{NLCD}$ also shows that the paddy rice area in these two products is consistent with each other (Fig. 9c).

The total area of paddy rice fields in the $Rice_{Landsat}$ map and $Rice_{NLCD}$ product is 2517 km^2 and 3309 km^2, respectively. We calculated the paddy rice area in the four counties of the study area from the $Rice_{Landsat}$ map and $Rice_{NLCD}$ product (Fig. 10a). $Rice_{NLCD}$ has more paddy rice area than $Rice_{Landsat}$ in all counties with the largest difference in Dawa County. The frequency distribution of the differences between $Rice_{Landsat}$ and $Rice_{NLCD}$ shows that more than 50% of pixels have the same percentage fraction of paddy rice area in the 1 km × 1 km pixel (Fig. 10b). 80% of pixels are located in the range of ±20%, which means the percentage fraction of paddy rice in most pixels from $Rice_{Landsat}$ and $Rice_{NLCD}$ agreed with each other. More negative than positive difference percentage values also indicates that the estimated paddy rice area in $Rice_{NLCD}$ is greater than that of $Rice_{Landsat}$. The visualization and digitalization process may introduce some error since producers might have different criteria.

The paddy rice area in Panjin City in the $Rice_{Landsat}$ map was higher than the statistical data (1373 km^2 versus 1076 km^2). The uncertainty of statistical data (artificial error or omission) between the $Rice_{Landsat}$ map and the statistical data might contribute to the difference. Since the statistical yearbook in Liaoning province in 2014 was the from the sample survey, it might not be able to represent the whole area condition.

Another study showed that paddy rice area in Panjin City is 1832 km^2 in 2010 using MODIS data (Zhang et al., 2015). It is higher than both the statistical data and our results. However, the different observation time might explain the difference. Another possible reason might be the natural wetlands used in this study was not very accurate and some of the natural wetlands were misclassified as paddy rice.

We also compared the paddy rice map derived from the pixel- and phenology-based algorithm with paddy rice maps derived from other two conventional classification methods (the image-based clustering methods), ISODATA and Support Vector Machine (SVM), using the image in DOY 159 (paddy rice flooding period, Fig. S1). The paddy rice map from the ISODATA showed more fragmented paddy rice area (Fig. S2) than our results. The overall accuracy and Kappa coefficient are 84%, and 0.64, respectively. Both the producer's and user's accuracy are 76% (Table S1). The overall accuracy and Kappa coefficient for SVM method are 94% and 0.87, very close to our results. However, a big area of water body in the northern part is misclassified as paddy rice (Fig. S3). The producer's accuracy is even higher than ours (96% vs. 93%) (Table S2). That is because no sample sites were located in the misclassified area. The pixel- and phenology-based paddy rice map showed higher accuracy than the ISODATA method and does not need the training samples, yet the SVM needs extensive field samples to build the prior-knowledge.

4.3. Sources of uncertainty and limitation

Malfunctions of the satellite and operation of sensors may reduce the availability of data. In this study, we missed three images for the study area not scanned by the Landsat 8 OLI sensor. The data quality is also constrained by cloud and cloud shadow. If there is no available image during the flooding period of paddy rice because of the acquisition schedule or cloud, it is hard to map paddy rice using any algorithm based on optical remote sensing. The irrigation or flooding event in other land cover types during the paddy rice flooding/transplanting period might affect the classification results. The mixed pixels of rice paddy fields and non-rice paddy fields (roads, irrigation channel, etc.) might be missed if the flooding signal is not captured. The combination of the Landsat 7 (ETM+) and Landsat 8 (OLI) imagery could potentially provide data at eight-day intervals which may increase the data availability for phenology-based paddy rice mapping (Qin et al., 2015). However, the stripe present in Landsat 7 images could spoil the results even part of it is correctable. MODIS LST products were used to choose the images during the flooding period for identifying paddy rice areas. However, there is no LST product from the Landsat series. The temperature-defined plant growing season depicted well the growing stages of paddy rice in temperate zones. However, the relationship between LST dynamics and the paddy rice growing season at the pixel level might be different at the regional level.

4.4. Future work and challenges

MODIS data (MOD09A1) have the advantage of higher temporal resolution (8 days) than Landsat 8 (16 days), which increases its ability to capture the flooding period. However, the lower spatial resolution of MODIS data (500 m versus Landsat 8's 30 m) presents the problem of mixed pixels in fragmented areas where paddy rice plots are smaller than 500 m. Combining of MODIS data and Landsat 8 data is a potential solution to improve the accuracy and spatial resolution of paddy rice mapping (Wang et al., 2015). The

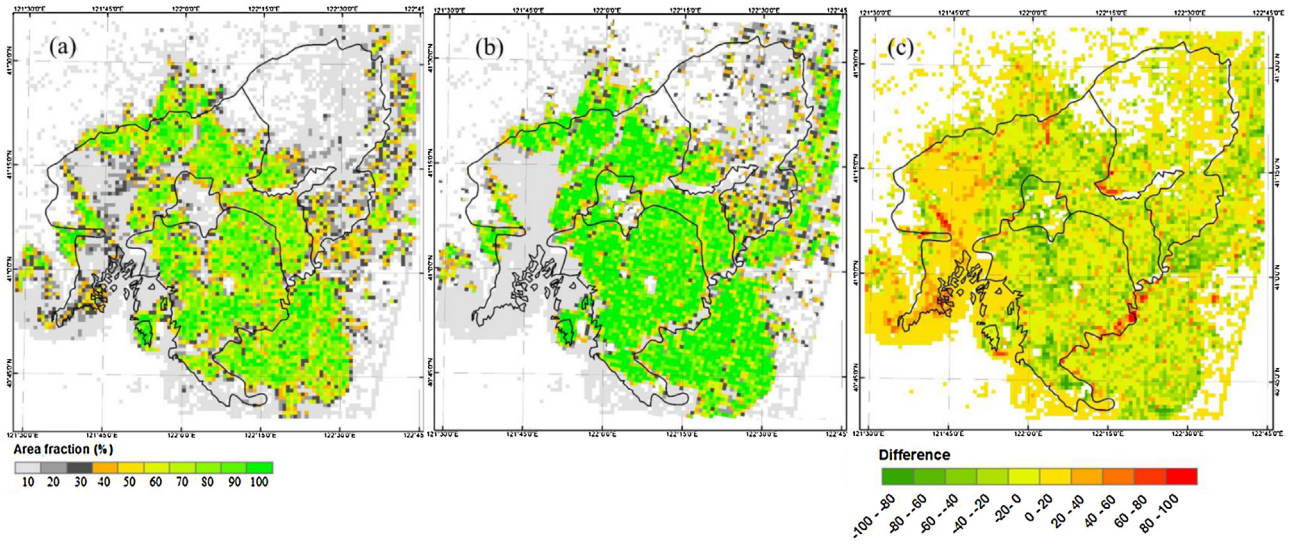

Fig. 9. Paddy rice maps derived from (a) the $Rice_{Landsat}$ and (b) the $Rice_{NLCD}$ at the 1-km spatial resolution (c) the comparison between the $Rice_{Landsat}$ and the $Rice_{NLCD}$.

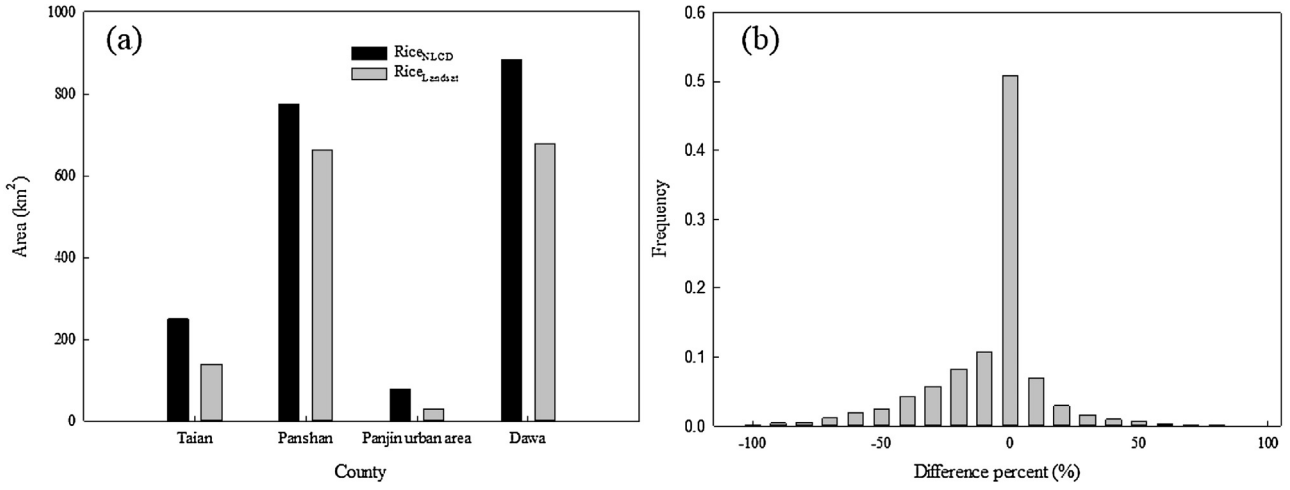

Fig. 10. The quantitative comparison between paddy rice maps derived from the $Rice_{Landsat}$ and the $Rice_{NLCD}$ at (a) county level and (b) pixel level.

phenology-based paddy rice mapping algorithm, developed in the temperate region with complex landscapes of paddy rice and natural wetland, has the potential to be applied in areas with similar climate system and ecosystems, which can provide more accurate paddy rice map for food production, water resource management, and methane emission estimation. There is still a need to develop a more accurate Landsat and/or MODIS based natural wetland mask in the future to further improve the accuracy of the paddy rice mapping.

Cloud and cloud shadow with the flooding feature of a high water-related index (LSWI) are identified as flooding pixels and may affect paddy rice mapping. Improved cloud and cloud shadow algorithms can be used to reduce their residual contamination. The combination of optical and radar sensors is a way to take advantage of both optical and radar remote sensing in order to map paddy rice (Yang et al., 2008; Zhang et al., 2009).

The selection of images in the flooding period was based on the crop calendar, local weather data, and LST data from MODIS. Local crop calendar and weather data are difficult to collect and might not be enough to reflect the regional conditions. LST data from satellites can be used to support image selection in large area paddy rice mapping. The relationship between LST dynamics and the paddy rice growing season needs to be investigated in different climate zones. Extreme weather events, including delays of temperature in spring and flooding events during the paddy rice flooding/transplanting period, raise several more challenges to paddy rice mapping.

5. Conclusion

This study aimed to use MODIS and Landsat 8 imagery to map paddy rice in the Panjin Plain, Northeastern China, which represents our continual efforts to provide more accurate and updated paddy rice maps by studying unique spectral features of the rice crop system. We generated the paddy rice map of the Panjin Plain at a 30 m spatial resolution based on the pixel- and phenology-based algorithm in a region with a coexistent paddy rice and wetland landscape. The validation tests indicated the high accuracy of our paddy rice map. Comparison of this map with other paddy rice products yielded high levels of consistency and revealed that this map provided more detailed information about the distribution of paddy rice areas because of its higher spatial resolution. The resultant paddy rice map might be affected by the data availability and quality (cloud and cloud shadow) during the critical plant growing stage (flooding/inundation). With the improvement of cloud and cloud shadow detection and LST retrieval from Landsat 8, it has great potential to provide reliable, sustainable data for paddy rice

mapping in the future. The combination of Landsat 7, 8, and MODIS imagery can open up many more possibilities for the mapping of paddy rice in complex landscapes.

Acknowledgements

This study was supported in part by research grants from the National Aeronautics and Space Administration (NASA) Land Cover and Land Use Change program (NNX11AJ35G), the National Science Foundation (NSF) EPSCoR program (NSF-0919466), National Institutes of Health (NIH) FIC (1R56TW009502-01) and NIAID (1R01AI101028-01AI). We would like to thank Sarah Xiao at Yale University for English editing of the manuscript.

Appendix A. Supplementary data

Supplementary data associated with this article can be found, in the online version, at http://dx.doi.org/10.1016/j.jag.2015.11.001.

References

Adler-Golden, S.M., Matthew, M.W., Bernstein, L.S., Levine, R.Y., Berk, A., Richtsmeier, S.C., Acharya, P.K., Anderson, G.P., Felde, G., Gardner, J., 1999. Atmospheric correction for short-wave spectral imagery based on MODTRAN 4. Proceedings SPIE Intetnational Society Optical Engineering, 61–69.

Beddington, J., Asaduzzaman, M., Clark, M., 2012. Achieving food security in the face of climate change: Final report from the Commission on Sustainable Agriculture and Climate Change.

Bouman, B., Tuong, T.P., 2001. Field water management to save water and increase its productivity in irrigated lowland rice. Agric. Water Manag. 49, 11–30.

Brisco, B., Li, K., Tedford, B., Charbonneau, F., Yun, S., Murnaghan, K., 2012. Compact polarimetry assessment for rice and wetland mapping. Int. J. Remote Sens. 34, 1949–1964.

Döll, P., 2002. Impact of climate change and variability on irrigation requirements: a global perspective. Clim. Change 54, 269–293.

Dong, J., Xiao, X., Sheldon, S., Biradar, C., Duong, N.D., Hazarika, M., 2012a. A comparison of forest cover maps in Mainland Southeast Asia from multiple sources: PALSAR, MERIS, MODIS and FRA. Remote Sens. Environ. 127, 60–73.

Dong, J., Xiao, X., Sheldon, S., Biradar, C., Xie, G., 2012b. Mapping tropical forests and rubber plantations in complex landscapes by integrating PALSAR and MODIS imagery. ISPRS J. Photogramm. Remote Sens. 74, 20–33.

Dong, J., Xiao, X., Sheldon, S., Biradar, C., Zhang, G., Duong, N.D., Hazarika, M., Wikantika, K., Takeuhci, W., Moore III, B., 2014. A 50-m Forest Cover Map in Southeast Asia from ALOS/PALSAR and Its Application on Forest Fragmentation Assessment. PloS one, 9, e85801.

FAO, 2013. Statistical Yearbook 2013: World Food and Agriculture. FAO (Food and Agriculture Organziation of the United Nations), Rome.

Godfray, H.C.J., Beddington, J.R., Crute, I.R., Haddad, L., Lawrence, D., Muir, J.F., Pretty, J., Robinson, S., Thomas, S.M., Toulmin, C., 2010. Food security: the challenge of feeding 9 billion people. Science 327, 812–818.

Gong, P., Niu, Z., Cheng, X., Zhao, K., Zhou, D., Guo, J., Liang, L., Wang, X., Li, D., Huang, H., 2010. China's wetland change (1990–2000) determined by remote sensing. Sci. China Earth Sci. 53, 1036–1042.

Hall, D.K., Riggs, G.A., Salomonson, V.V., DiGirolamo, N.E., Bayr, K.J., 2002. MODIS snow-cover products. Remote Sens. Environ. 83, 181–194.

Huete, A., Didan, K., Miura, T., Rodriguez, E.P., Gao, X., Ferreira, L.G., 2002. Overview of the radiometric and biophysical performance of the MODIS vegetation indices. Remote Sens. Environ. 83, 195–213.

IPCC (2013). Climate Change 2013: The Physical Science Basis, Contribution of Working Group I Contribution to the Fifth Assessment Report of Intergovernmental Panel on Climate.

Jin, C., Xiao, X., Dong, J., Qin, Y., Wang, Z., 2015. Mapping paddy rice distribution using multi-temporal Landsat imagery in the Sanjiang Plain, northeast China. Front. Earth Sci., 1–14.

Li, R.P., Liu, X.M., Zhou, G.S., 2006. The characteristics of Phragmites phenology in Panjin wetland and its responses to climate change. J. Meteorol. Environ. 22, 30–34.

Liaoning Statistical Bureau, 2013. Liaoning Statistical Yearbook in 2013. China Statistical Press.

Liaoning Statistical Bureau, 2014. Liaoning Statistical Yearbook in 2014. China Statistical Press.

Liu, J., Kuang, W., Zhang, Z., Xu, X., Qin, Y., Ning, J., Zhou, W., Zhang, S., Li, R., Yan, C., Wu, S., Shi, X., Jiang, N., Yu, D., Pan, X., Chi, W., 2014. Spatiotemporal characteristics, patterns, and causes of land-use changes in China since the late 1980. J. Geog. Sci. 24, 195–210.

Liu, J., Liu, M., Tian, H., Zhuang, D., Zhang, Z., Zhang, W., Tang, X., Deng, X., 2005. Spatial and temporal patterns of China's cropland during 1990–2000: an analysis based on Landsat TM data. Remote Sens. Environ. 98, 442–456.

Matthew, M.W., Adler-Golden, S.M., Berk, A., Richtsmeier, S.C., Levine, R.Y., Bernstein, L.S., Acharya, P.K., Anderson, G.P., Felde, G.W., Hoke, M.L., 2000. Status of atmospheric correction using a MODTRAN4-based algorithm. In: AeroSense 2000. International Society for Optics and Photonics, pp. 199–207.

Matthews, R., Wassmann, R., Knox, J., Buendia, L., 2001. Using a crop/soil simulation model and GIS techniques to assess methane emissions from rice fields in Asia. IV. Upscaling to national levels. In: Methane Emissions from Major Rice Ecosystems in Asia. Springer, pp. 201–217.

Qin, Y., Xiao, X., Dong, J., Zhou, Y., Zhu, Z., Zhang, G., Du, G., Jin, C., Kou, W., Wang, J., Li, X., 2015. Mapping paddy rice planting area in cold temperate climate region through analysis of time series Landsat 8 (OLI), Landsat 7 (ETM+) and MODIS imagery. ISPRS J. Photogramm. Remote Sens. 105, 220–233.

Salmon J.M., Friedl M.A., Frolking S., Wisser D., Douglas E.M., 2015. Global rain-fed, irrigated, and paddy croplands A new high resolution map derived from remote sensing, crop inventories and climate data, International Journal of Applied Earth Observation and Geoinformation, 38, 321–334.

Stocker, T.F., Dahe, Q., Plattner, G.-K., 2013. Climate Change 2013: The Physical Science Basis. Working Group I Contribution to the Fifth Assessment Report of the Intergovernmental Panel on Climate Change. Summary for Policymakers (IPCC, 2013).

Wan, Z., Zhang, Y., Zhang, Q., Li, Z.-l, 2002. Validation of the land-surface temperature products retrieved from Terra Moderate Resolution Imaging Spectroradiometer data. Remote Sens. Environ. 83, 163–180.

Wang, J., Xiao, X., Qin, Y., Dong, J., Zhang, G., Kou, W., Jin, C., Zhou, Y., Zhang, Y., 2015. Mapping paddy rice planting area in wheat-rice double-cropped areas through integration of Landsat-8 OLI, MODIS, and PALSAR images. Sci. Rep. 5.

Xiao, X., Boles, S., Frolking, S., Salas, W., Moore, B., Li, C., He, L., Zhao, R., 2002a. Observation of flooding and rice transplanting of paddy rice fields at the site to landscape scales in China using VEGETATION sensor data. Int. J. Remote Sens. 23, 3009–3022.

Xiao, X., Boles, S., Frolking, S., Salas, W., Moore Iii, B., Li, C., He, L., Zhao, R., 2002b. Landscape-scale characterization of cropland in China using Vegetation and Landsat TM images. Int. J. Remote Sens. 23, 3579–3594.

Xiao, X.M., Boles, S., Frolking, S., Li, C.S., Babu, J.Y., Salas, W., Moore, B., 2006. Mapping paddy rice agriculture in South and Southeast Asia using multi-temporal MODIS images. Remote Sens. Environ. 100, 95–113.

Xiao, X.M., Boles, S., Liu, J.Y., Zhuang, D.F., Frolking, S., Li, C.S., Salas, W., Moore, B., 2005. Mapping paddy rice agriculture in southern China using multi-temporal MODIS images. Remote Sens. Environ. 95, 480–492.

Xu, L., Zhang, Y., Pengshi, C., Mao, L., 2009. Analysis on the changing characteristics and influencing factors of panjin wetland during the past 20 years [J]. J. Nat. Resour. 24, 483–490.

Yang, S.B., Shen, S.H., Li, B.B., Le Toan, T., He, W., 2008. Rice mapping and monitoring using ENVISAT ASAR data. IEEE Geosci. Remote Sens. Lett. 5, 108–112.

Yu, X.F., Zhuang, D.F., 2006. Monitoring forest phenophases of Northeast China based on MODIS NDVI data. Resour. Sci. 28, 111–117.

Zhang, G., Xiao, X., Dong, J., Kou, W., Jin, C., Qin, Y., Zhou, Y., Wang, J., Menarguez, M.A., Biradar, C., 2015. Mapping paddy rice planting areas through time series analysis of MODIS land surface temperature and vegetation index data. ISPRS J. Photogramm. Remote Sens. 106, 157–171.

Zhang, Y., Wang, C., Wu, J., Qi, J., Salas, W.A., 2009. Mapping paddy rice with multitemporal ALOS/PALSAR imagery in southeast China. Int. J. Remote Sens. 30, 6301–6315.

Zhang, Z., Wang, X., Zhao, X., Liu, B., Yi, L., Zuo, L., Wen, Q., Liu, F., Xu, J., Hu, S., 2014. A 2010 update of national land use/cover database of China at 1:100000 scale using medium spatial resolution satellite images. Remote Sens. Environ. 149, 142–154.

Zhuang, Q., Melack, J.M., Zimov, S., Walter, K.M., Butenhoff, C.L., Khalil, M.A.K., 2009. Global methan emissions from wetlands, rice paddies, and lakes. EOS Trans. Am. Geophys. Union 90, 37–38.